Journal of Radioanalytical and Nuclear Chemistry (2023) 332:1935–1952
https://doi.org/10.1007/s10967-023-08862-z

Novel nano *Rosmarinus officinalis* phytomass adsorbent for strontium and europium removal from aqueous solution: batch and packet techniques

Maha A. Youssef[1] · **Lamis A. Attia**[2]

Received: 16 December 2022 / Accepted: 6 March 2023 / Published online: 18 March 2023

Abstract
Phytomass sorbent material (RM) was obtained as a by-product from the process of essential oil extraction. Its phosphoric acid-modified nano-form, N-RM, was used to absorb Sr(II) and Eu(III) from an aqueous solution. The pseudo-second-order is the better fitting model. Isotherm Langmuir and Freundlich models were fitted with a maximum capacity of q_m 18.2, 60.4, 11.5, and 13.8 mg/g for Eu/RM, Eu/N-RM, Sr/RM, and Sr/N-RM, respectively. The packet technique promised to be applicable on a large scale for the treatment of contaminated water. Both RM and N-RM are effective eco-friendly adsorbents for the removal of Eu(III) and Sr(II).

Keywords Strontium · Europium · Rosemary · Adsorption

Introduction

Low and intermediate level radioactive wastes are generated in radiochemical laboratories, research reactors, radioisotopes of metallurgical laboratories, activation analysis units, nuclear medicine divisions in hospitals, universities, and research organizations, as well as in industrial activities [1, 2]. The radionuclides released may be transported with water, adsorbed by inorganic particulate matter, and/or deposited in bottom sediments, where they pose a threat to living beings. Radioactive strontium occurs in the environment as ^{89}Sr and ^{90}Sr with a half-life of 51 days and 29 years, respectively. ^{90}Sr, a soft emitter of energy with a 0.5460 MeV, is highly mobile and can migrate into the bottom layers of soil and into groundwater with percolating water. Because it is chemically similar to calcium it is easily integrated into the bone, where it damages blood-producing cells and continues to irradiate localized tissues, eventually leading to bone sarcoma and leukemia [3]. Where large amounts of elements are required, europium (as an analog) is frequently used to represent all trivalent actinides [4]. ^{152}Eu ($t_{1/2}$ = 13.54 years) and ^{154}Eu ($t_{1/2}$ = 8.67 years) are produced primarily in radioactive waste as fission products [5]. ^{152}Eu and ^{154}Eu can also be produced by neutron activation of nuclear reactor control rods ($^{151}\mathrm{Eu} \xrightarrow{n,\gamma} {}^{152}\mathrm{Eu}$). Sorption has been the subject of several studies as a process for treating contaminated water, allowing the removal of a large amount of water pollutants; additionally, this method has proven to be a highly effective and economical process [6, 7]. The presence of various active functional groups, like amino, hydroxyl, carboxylic acid, and carbonyl groups, etc., are the chief constituents including organic and inorganic components of phytomass [8], and thus they are apparently rich in carbon content for producing activated carbon powders. This adsorbent makes them available for chelation or complexation with metal ions. The leaves of the rosemary plant contain some lignocellulose material such as lignin, cellulose, hemicelluloses, and pectin, making them the most effective and least expensive phytomass material [9, 10]. Using carbonized *Rosmarinus officinalis* plants, Hg(II) was removed from the watered solution [11, 12]. The goal of this study was to look at the ability of RM and H_3PO_4 treated *Rosmarinus officinalis* leaves N-RM to adsorb Eu(III) and Sr(II) ions from an aqueous solution. The optimum condition was determined using the batch technique (pH, time,

✉ Maha A. Youssef
maha_hasa@yahoo.com

[1] Department of Analytical Chemistry and Control, Hot Laboratories Center, Egyptian Atomic Energy Authority, Cairo, Egypt

[2] Radiation Protection Department, Nuclear Research Center, Egyptian Atomic Energy Authority, P.O. Box 13759, Cairo, Egypt

and concentration effect). Different isotherm and kinetic models were applied to estimate the available reaction mechanism. At two different pH 2, and 5, the effect of interfering ions (Fe(III), Co(II), and Cr(III)) on the removal of Eu(III) and Sr(II) and their adsorption behavior was investigated. A new packet technique was applied for the best and easiest treatment application.

Materials and methods

Chemicals and material

Chemicals of analytical grade were used during this study without further purification; Eu_2O_3 and $SrCl_2$ were supplied by E. Merck. Cobalt (II), iron (III), and chromium (III) stock solutions were prepared from cobalt chloride, iron chloride, and chromium chloride. Double distilled water has been used in all experiments.

Instruments

The inductively coupled plasma (ICP-OES) 6 Wentworth Drive Hudson New Hampshire 03,051, USA was used to measure the concentration of Eu(III), Sr(II), and all interfering ions (Fe(III), Cr(III), and Co(II)). The chemical composition of the prepared sample was analyzed by the Energy Dispersive X-ray spectrometer EDX. The surface structure of synthetic material was examined by a scanning electron microscope (SEM) (JEOL, JSM-6510A, Japan). The size and morphology of N-RM nanoparticles were measured by TEM (Hitachi H-7100, Japan). Functional compositions of RM and N-RM have been examined with Fourier transform infrared (FTIR) spectroscopy (Thermo, USA). The thermal behavior of the prepared powder was carried out using TG–DTA (SDTQ600, TA Instruments, New Castle, DE, USA). The pH of the solution was measured with a Hitachi pH meter. The XRD examination was performed on a Shimadzu XRD–6100 with diffraction patterns created across a 2θ range of 10–80 using Cu K radiation (= 1.5406) and continuously scanned at a speed of 10/min with a sample pitch of 0.1 and a preset period of 0.6 s.

Experiments

Preparation of adsorbents

The crushed, de-oiled residue of rosemary leaves was obtained as a byproduct from the essential oil steam distillation extraction process (It is a multistage continuous distillation process where steam is used as a stripping gas to extract the oils. Steam is directed through the plant material. The mixture of hot vapors is collected and condensed in order to produce a liquid in which the oil and water form two distinct layers). This waste was rinsed with diluted nitric acid (0.1 M) in order to eliminate the color. The sample was washed with distilled water, dried, grinded, and sieved to the desired size of 20 mesh. Phosphoric acid was used as an activating agent in a ratio of 1:1(w: w) and heated at 110 °C for 2 h and at 500 °C for 4 h. The reason for using phosphoric acid as a chemical activating agent is to increase surface area. The mixture was then dried overnight at 105 °C. The activated product was then washed with deionized water several times to remove the excess acid until the pH of the solution reached almost neutral. The final product was kept in the oven for 12 h at a temperature of 60–80 °C to remove moisture.

Sorption studies

Sorption studies were conducted by batch technique and packet test using simulated waste water containing certain amounts of Eu(III) and Sr(II) (10 mL) and 0.1 g of adsorbent(RM and/or N-RM). Batch experiments were carried out to determine the adsorption isotherms of metal ions onto the adsorbents in 25 mL closed polypropylene vials. The vials were shaken at a constant rate, allowing sufficient time for adsorption equilibrium. The applied shaking speed was assumed to allow all of the surface area to come into contact with Eu(III) and Sr(II) ions during the experiments. The study was performed at room temperature to be representative of environmentally relevant conditions. The vials were plugged and kept closed to avoid the fluctuation of pH due to the exchange of gases during the experiment. The effects of various parameters on the rate of sorption process were observed by varying contact time (15–240 min.), metal ions concentration (50 − 400 mg/L), and pH of the solution (2–6). ICP-OES was used to determine the remaining concentrations of Eu(III) and Sr(II). The volume of the solution was held constant at 10 mL. The experimental results, throughout this work, were mathematically treated to calculate the removal percent (R%) and the number of ions adsorbed per gram of RM or N-RM at equilibrium (q_e) using the following Eq. 1 and2:

$$R\% = \frac{(C_i - C_f)}{C_i} \times 100 \quad (1)$$

$$q_e = \left(C_i - C_f\right) \times \frac{V}{M} \quad (2)$$

C_i and C_f are the initial and final concentrations of the studied metal ions; V is the volume of the solutions (0.01 L), and M is the mass of RM or N-RM (0.1 g).

Packets technique

The adsorption tests were carried out in packets (made of 100% high density polyethylene fibers) containing adsorbents RM and/or N-RM (0.1 g) and immersed in a vessel containing 20 mL of simulated waste water. The optimum conditions of pH (5), time (3 h) at room temperature were applied to the process. This experiment is useful in understanding and predicting the behaviour of the purification process and is easily applicable to large-scale effluent. Actually, the experiments were carried out by using five packets, two of which were filled with RM, the other two were filled with N-RM, and the remaining one was left empty without any adsorbents (blank) to investigate the availability of packet material adsorption. The first two packets (one vial contain RM and the other containing N-RM) were immersed in beakers containing a mixture of the investigated metal ions Eu(III) and Sr(II), while the other three packets were immersed in beakers containing a mixture of 20 ppm (Eu(III), Sr(II), Fe(III), Co(II), and Cr(III)). After 3 h, the packets were removed, and the remaining concentration of metal ions in the beaker was measured using ICP-OES.

Degree of selectivity and sorption affinity

The effects of interfering ions Fe(III), Co(II), and Cr(III) on the affinity of RM and N-RM materials for them, as well as their effects on the removal of Eu(III) and Sr(II) as interfering ions due to corrosion reactions in reactors, were also investigated. This is achieved by combining 10 mL of solution containing different concentrations (5, 10, and 20 mg/L of (Fe(III), Co(II), and Cr(III)), as well as constant concentration of Eu(III) and Sr(II) (20 mg/L) with 0.1 g of RM or N-RM and allowing it to stand for 3 h at room temperature 25 °C. The prepared solutions were fixed at two different pH values: 2 to ensure that all ions especially, Fe(III), Eu(III), and Cr(III) are dissolved, and 5 to estimate the highest removal % for all ions, especially Co(II) and Sr^{+2}.

Results and discussion

Characterization

The elemental analysis (EDS) pattern of the treated and untreated samples produced via heating and chemical treatment by phosphoric acid is shown in Fig. 1 and Table 1. After filling the RM with phosphoric acid, the weight and number of carbon and oxygen atoms both decreased. This confirms the interaction of phosphoric acid chemical species with the adsorbent surface. The phosphorus content of modified samples is higher than that of parent samples. The combination of physical and chemical treatment appears to have accelerated chemical changes in the material and enabled hydrogen and oxygen removal.

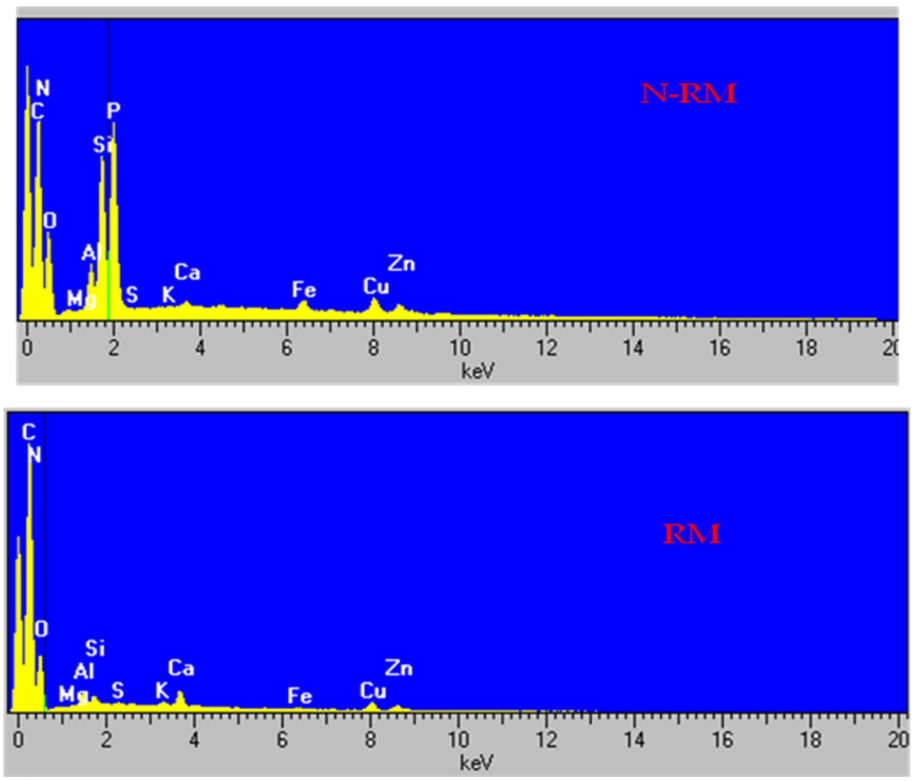

Fig. 1 EDX analysis for both RM and N-RM adsorbents

Table 1 Composition of RM and N-RM by EDS analysis

Element component	RM %	N-RM %
C	47.48	43.69
N	16.28	8.88
O	27.21	23.38
Mg	0.12	–
Al	0.87	1.64
Si	0.56	5.54
P	–	8.11
S	0.12	0.10
K	0.29	–
Ca	1.35	0.34
Fe	0.24	1.40
Cu	3.20	3.97
Zn	2.26	2.93

X-ray diffraction characterization (XRD) for RM and N-RM were shown in Fig. 2. Both the samples present two large diffraction peaks around 20–30° and 15–25°, characteristic of amorphous carbonaceous materials. The two peaks confirm the disordered nature and also the amorphous and graphitic features of both samples. The graphitic structures are associated with the bond breaking of the organic components in the phytomass precursors. The diffuse scattering of disordered amorphous carbon provides a significant full width and half maximum (FWHM), confirming the amorphous character of AC (N-RM) [13].

A transmission electron microscope (TEM) was used for N-RM, which allows for direct imaging of the atomic structure of the material. The information obtained from TEM is useful for studying the atomic structure, lattice spacing, and crystal symmetry. (Fig. 3a) shows several huge amounts of carbon nanotubes (CNT) in the diameter range of 10.7—22.4 nm. Other shapes of large and small black spots in CNT aggregates are shown in Fig. 3b, d. Figure 3c shows the internal structure with a small portion of phosphorous. One can also observe a thin outer layer of amorphous carbon which covers it. Carbon nanoparticles identical to those produced by ablating candle soot and graphite powder with a laser were found in the majority of the samples [14].

The SEM images were taken at a magnification of 1000 × before adsorption and 500 after adsorption. There were only cylindrical structures present, with homogeneous and condensed parts reflecting the presence of different functional groups on the surface of the raw RM adsorbent. However, after chemical modification, the N-RM displayed large primary pores and smaller secondary pores inside the primary pores, as well as a change in surface shape from cylindrical to multilayer, which increased the ability of Eu(III) and Sr(II) to interact chemically with the interlayer function groups (Fig. 4). Also pores on the surface of RM can participate in the removal of Eu(III) and Sr (II). As a result, the removal affinity of N-RM for Eu(III) and Sr(II) may be greater than that of inactivated RM.

FT-IR spectroscopy: The chemical composition of a material can be determined using infrared spectroscopy. As shown in Fig. 5, the surface functional groups of RM and N-RM adsorbents are investigated before and after Eu(III) and Sr(II) loading. The following characteristic peaks appeared after analysis. At 1700–1730 cm^{-1}, the most noticeable changes on the surface of the RM and N-RM adsorbents before Eu(III) and Sr(II) adsorption are observed. The stretching vibrations of Coo^{-}groups on the edges of layer planes or conjugated carbonyl groups

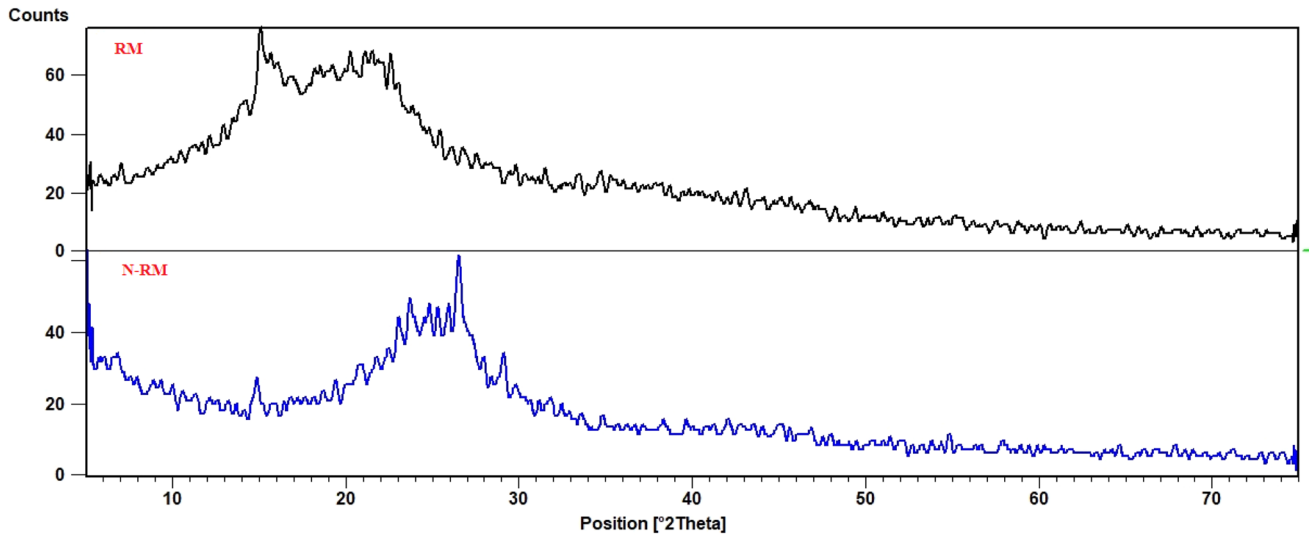

Fig. 2 XRD analysis for both RM and N-RM adsorbents

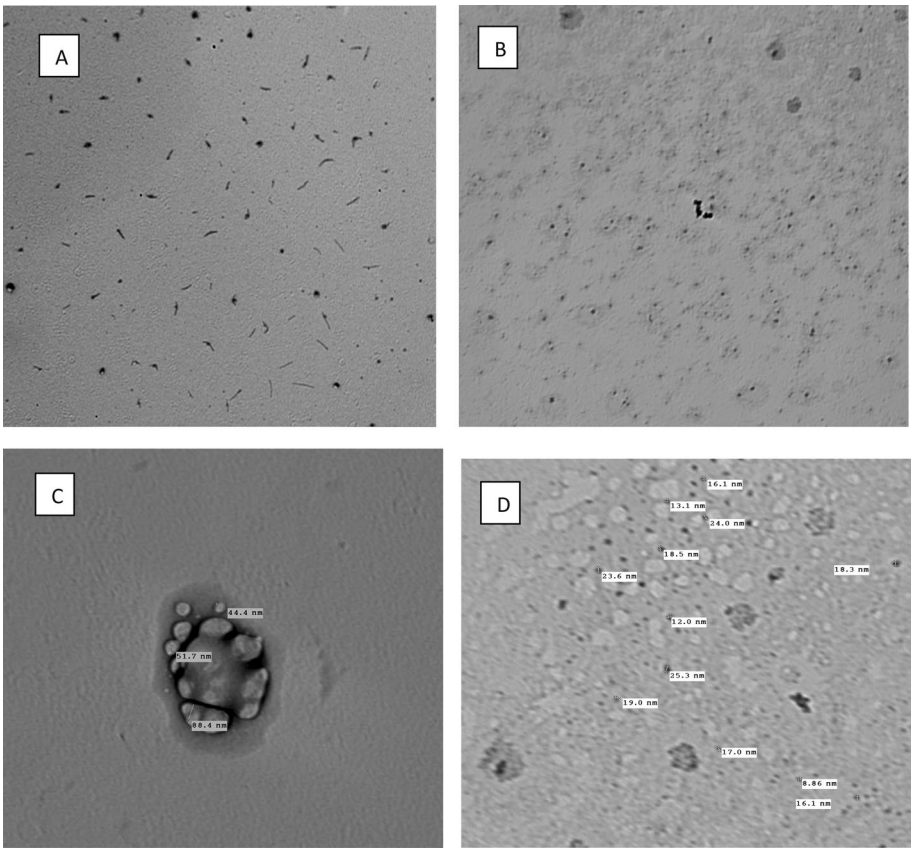

Fig. 3 Transmission electron microscope analysis (TEM) for N-RM

(C–O in carboxylic acid and lactone groups) are associated with the band centered at 1731 cm^{-1}[15]. The spectrum of the acid-treated adsorbent shows a significant change in this band, showing the effect of phosphoric acid on the rosemary leave. The broadband between 1300 and 900 cm^{-1} in acid treated rosemary leave has a maximum of 1070–1080 cm^{-1}[15]. Phosphorus and phosphoric carbonaceous substances have a distinctive absorption in this area. The ionized linkage $P^{+}O^{-}$ in acid phosphate esters and symmetrical vibration in a P–O–P (polyphosphate) chain are responsible for the peak at 1057–1033 cm^{-1} [15]. Besides the peak between 920 and 1000 cm^{-1}, corresponding to the POH bond, the band at 2360 cm^{-1}, corresponding to the PH bond, and the band at ~1240 cm^{-1} corresponding to the P–O bond, were also observed [16]. The spectra, therefore, suggest the formation of P-containing carbonaceous structures like acid phosphates and polyphosphates in phosphoric acid-activated rosemary leaves [15]. It also demonstrates that the peaks at 3420.6 cm^{-1}, 2928.1 cm^{-1}, and 1095.8 cm^{-1} are reduced to 3411.5 cm^{-1}, 2921.5 cm^{-1}, and 1091.5 cm^{-1}, respectively, after adsorption of Eu(III) and/or Sr(II). This resulted in the surface functional groups of H_3PO_4-treated rosemary leaves combining intensively with Eu(III) and/or Sr(II), and these groups have been shown to improve metal ion adsorption [17].

TGA–DTA thermal analysis obtained in an oxidizing atmosphere of dry air was used to study the thermal stability of the materials after the activation process (Fig. 6). It is important to indicate that at the beginning of the test, the mass loss is zero and the mass of the sample is 100%. The tests were performed by heating dry air from around 23 °C to 600 °C at a rate of 10 °C per min. Three steps of weight loss were observed for the RM sample. It was observed that the first stage included a slow mass loss of 10.25% due to the evaporation of water molecules, and it was from 31 °C to 250 °C. This is confirmed by the two small DTA endothermic peaks observed at T < 200 °C. The second stage was observed in the range of 250–380 °C with a weight loss of 45.116% due to the decomposition or degradation of cellulose and hemicelluloses, the structural components of organic material, and the change in slope of TGA to an arc shape. The third stage was found at temperatures between 380 and 600 degrees Celsius, with a weight loss due to the total oxidation of the materials. RM's overall weight loss was discovered to be 79.7235%.

The TGA for N-RM has only two stages: the first stage in the range of temperatures 30–250 °C is due to the lack of physically adsorbed water upon substance, which most likely occurred during storage, and the second step in the temperature range of 250–600 °C is due to surface groups formed during the activation process, along with carbon

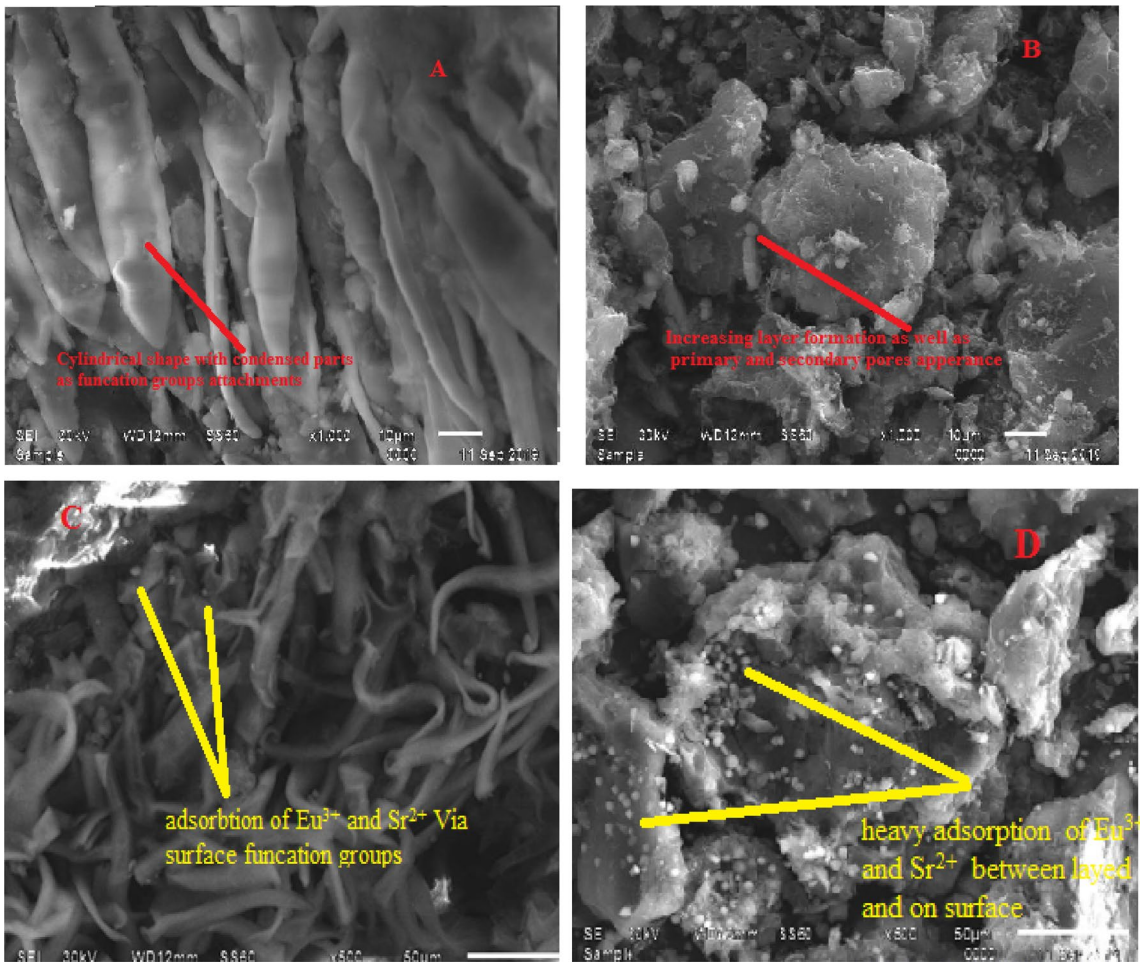

Fig. 4 SEM images of **A** RM, **B** N-RM, **C** RM- Eu(III)/Sr(II), **D** N- RM- Eu(III)/Sr(II) surfaces

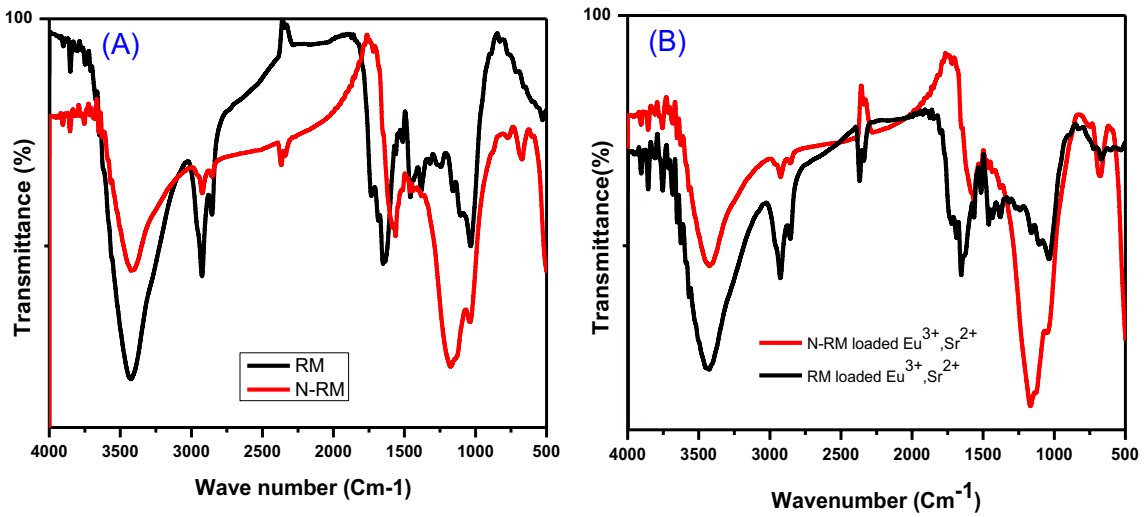

Fig. 5 Infrared spectrum of **A** RM and it modified form N- RM, **B** RM and N-RM loaded with Eu(III), Sr(II)

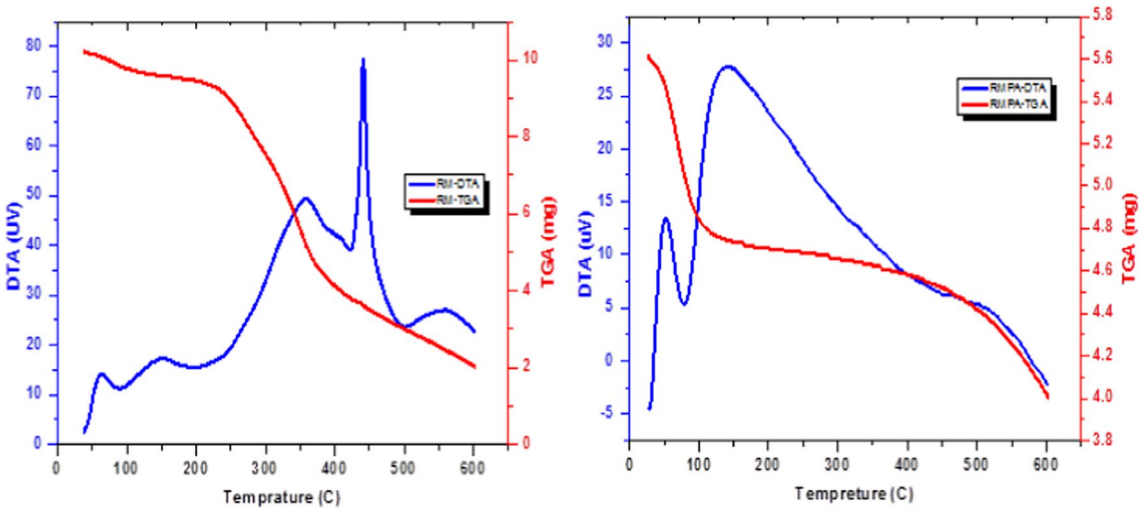

Fig. 6 Thermal analysis (DTA and TGA) of both RM and N-RM

skeleton decomposition and a weight loss of 13.039%. The total weight loss was found to be 28.0%. In addition, it can be discovered that the N-RM samples have similar decomposition profiles in the TGA curves with intense exothermic peaks (DTA) related to the thermal decomposition of organic matter, so that the penultimate mass loss phases, which overlap, can likewise be linked to the carbon N-RM's skeleton [18].

Adsorption factors

pH effect

The adsorption of strontium (II) and europium (III) onto the RM and N-RM was studied in the pH range from 2 to 6, and the results obtained are shown in Fig. 7. The uptake of Sr (II) and Eu (III) on the RM and N-RM is low at pH 2 and increases as the pH rises, except for the elimination of Eu(III) using N-RM, where the modification process increases the stability of the adsorbent and is unaffected by changes in pH (94 to 97 percent during pH 2 to 6). At pH 4, The maximum removal percentage for Eu(III) (83 and 97% for RM and N-RM, respectively) were achieved. The maximum removal percentage for Sr (II) was obtained at pH 6 (27 and 47% for RM and N-RM, respectively).

Because hydrogen ions in the acidic solution compete with metal ions at low pH values, metal ion adsorption is modest at low pH values, and adsorption increases as the pH value rises. The uptake of Eu(III) by the adsorbent at different pH values is also affected by the Eu(III) species. At pH

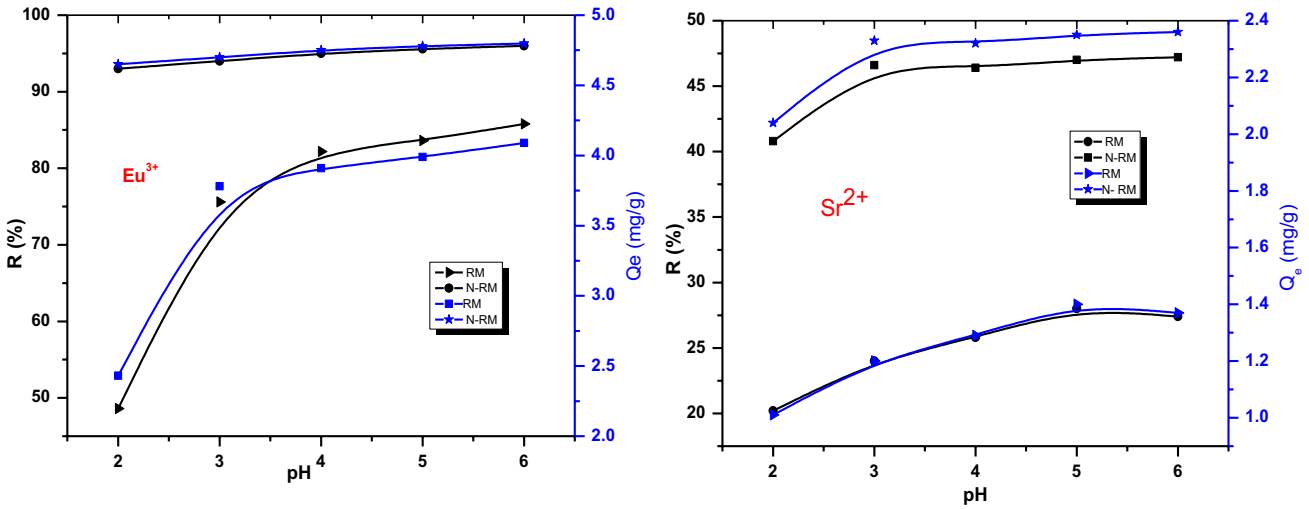

Fig. 7 The effect of pH on the removal % (as well as maximum capacity) of Sr(II) and Eu(III) using RM and N-RM at 25 °C and 50 mg/g

6, Eu(III) is the dominant species; it is reasonable to expect Eu(III) sorption to increase as pH increases. Both positively charged $Eu(OH)^{2+}$ and $Eu(OH)^{2+}$ are found in the pH ranges of 5–9 and 6.5–9.5, respectively. According to this evidence, in the initial pH range 1–5, the electric attraction of Eu(III) ions onto the surface of Rosmarinus and its nano-modified form is a preferred sorption mechanism, whereas precipitation of Eu(III) is the dominant process. Over pH 5, the species $Eu(OH)^{2+}$ and $Eu(OH)^{+}_{2}$ could also be retained on the sorbent surface[19, 20] Adsorption of both metal ions may be related to the exchange reaction with the functional groups of the resources of H^+ ions, like the COOH and OH groups. At the same time, at pH levels up to 6, Sr(II) is the dominant species, with little competition from H^+. Adsorbent materials have a higher affinity for trivalent metal ions (Eu(III) = 98%) than for divalent metal ions (Sr(II) = 48%), as shown in Fig. 7. As a result, the prepared N-RM nanomaterial is a promising solid phase for separating Eu(III) from all divalent metal ions, particularly Sr(II). The pH 5 solutions were chosen for further experiments and research on the spontaneous removal of Eu(III) and Sr(II) metal ions. The maximum capacity q_e of the prepared materials towards the investigated metal ions was evaluated at different pH ranges (2–6) and a constant concentration of 50 mg/L (Fig. 7). It was found that maximum capacity increased with increasing pH values. In the case of N-RM, q_e for of Eu(III) and Sr(II) at an initial concentration of 50 mg/L is 4.8 and 2.3 mg/g, respectively.

Mechanism of interaction

In generally, Eu(III) and Sr(II) can be immobilized into the mesoporous channels of RM via weak physical adsorptions, such as hydrogen bonding, hydrophobic attraction, or electrostatic interaction, or via covalent linkage inside the mesoporous channels on reactive OH groups in the prepared materials such as aldehyde, epoxide, and thiol groups [21]. Because the presence of the OH group, the expected mechanism for the adsorption of Eu(III) and Sr(II) using RM is an ion exchange reaction, as shown in the equation.

$$3RM - OH + Eu^{+3} \rightarrow -3RM - OEu + 3H^{+}$$

$$2RM - OH + Sr^{+2} \rightarrow 2RM - OSr + 2H^{+}$$

The modification of the Rose Mary (RM) surface using phosphoric acid makes its behavior in the elimination of europium and strontium is proactive, though increasing its removal %, capacity, and reduction in equilibrium time required, achieving an excellent goal of treatment. This may be related to several reasons; the phosphate groups show typical lewis-base properties in a wide pH range. By electrostatic contact or chelation, the phosphate groups on the RM surface can interact with both Eu (III) and Sr (II) [21]. According to *Varnali and Tiiziim-~algan 1995,* when M^+ interacts with a phosphate group, the phosphate group donates an electron to the cation, partially neutralizing the phosphate group charge. Furthermore, the M^{+}'s proclivity to form partial covalent bonds with phosphate oxygen may play a significant role in their attraction to the surface of RM. Significant charge transfer cations appear to have three important effects on the phosphate group: (1) a significant change in the O_1–P–O_2 bond angle; (2) a significant atomic charge redistribution (decrease in negative charge on RM and anionic oxygen atoms); (3) a significant change in the bond density (strengthening of the phosphate ester oxygen bond and weakening of the phosphate-anionic oxygen bonds) [22]. Iftekhar et al. (2018), explained that phosphoric acid is attached to the surface of the adsorbent via two expected mechanisms: electrostatic attraction or complexation as shown in Scheme 1. In the absence of metal ions, the preferred bath method for the phosphate group is the formation of phosphate monoesters [23].

Effect of contact time

The adsorption of europium and strontium on RM and N-RM was studied as a function of contact time in the range of 15–240 min. The removal percentage of Eu(III) and Sr(II) on N-RM was homogenous, very fast and did not change during all time range. This means that the number of sites available for Sr(II) and Eu (III) is significantly higher than the concentration used. The equilibrium was reached within 15 min. The efficient R% are reached up to 95 and 46% for Eu(III) and Sr(II), respectively. The adsorption of Eu(III) and Sr(II) on RM is a heterogeneous process with an initial rapid adsorption rate followed by a slower uptake. The adsorption process achieved equilibrium after 60 min with R% reach to about 85 and 27% for Eu(III) and Sr(II) respectively, as shown in Fig. 8. It is clear that modifying RM with phosphoric acid not only improves stability across all pH ranges but also reduces the time required to reach equilibrium (fast reaction). The data indicate that there is no significant change in the distribution ratio after this time up to 240 min. The main reason for increasing R% with time is the number of vacant adsorption sites on the adsorbent surface, and the adsorption eventually reached equilibrium because Eu(III) and Sr(II) occupied all of the adsorption sites. In comparison to the RM, the N-RM stiff and parallel-porous structure, as well as its appropriate pore size is responsible for its rapid removal rate.

Kinetic modeling

The majority of sorption processes involve three steps: (i) diffusion across the liquid layer enveloping the solid

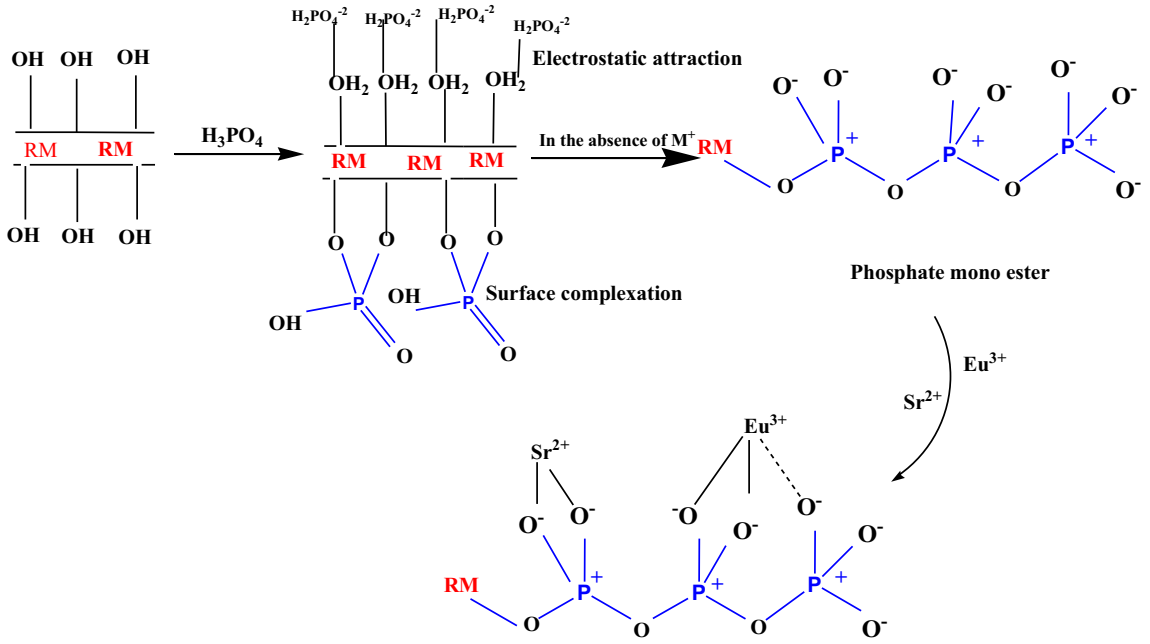

Scheme 1 Phosphoric acid reaction mechanism with RM surface, as well as Sr(II) and Eu(III)

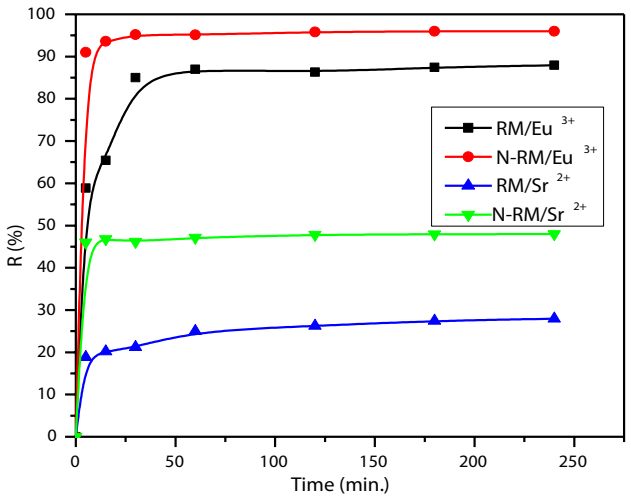

Fig. 8 The effect of contact time on the removal% of Eu(III)/Sr(II) using RM and N-RM

particles, (ii) propagation within the particle (posing a pore diffusion mechanism), and (iii) physical or chemical adsorption at active sites [24]. The transient behavior of the batch sorption process of each studied metal ion was analyzed using the Lagergren first-order kinetics model and the pseudo-second-order model [25, 26]. The Lagergren first-order and pseudo- second-order models were given by Eqs. 3 and 4 respectively and intraparticle diffusion kinetic model Eq. 5 [26]. The Elovish kinetic equation [27] was also shown in Eq. 6.

$$\log\left(q_e - q_t\right) = \log q_e - \left(\frac{K_1}{2.303}\right)t \tag{3}$$

$$\frac{t}{q_t} = \frac{1}{K_2 q_e^2} + \frac{t}{q_t} \tag{4}$$

$$q_t = K_p t^{1/2} + C \tag{5}$$

$$q_t = \left(\frac{1}{3}\right)\ln\alpha\beta + \left(\frac{1}{3}\right)\ln t \tag{6}$$

where k_1 is the rate constant of pseudo-first-order sorption (h^{-1}), q_e and q_t are mounts of metal adsorbed per gram of RM/N-RM (mg/g) at equilibrium and any time t, respectively. k_2 (g /mg hour) is the rate constant for pseudo-second-order adsorption. The constant of the intra-particle diffusion equation is k_p (mg g^{-1} $min^{-0.5}$), which can be obtained from the slope of the plot of q_t (mg g^{-1}) versus $t^{0.5}$. The influence of the boundary layer is reflected in the intercept "C". In the rate-controlling phase, the bigger the "C" value, the more critical surface adsorption is. When the intra-particle rate constants are high, this indicates that the rate of adsorbate sorption has improved. If intra-particle diffusion is the rate-limiting phase in this model, plotting q_t against $t^{0.5}$ should result in a straight line crossing the origin. The initial sorption rate and the desorption constant associated with

the degree of surface saturation and activation energy for chemical adsorption are represented by Elovich coefficients of α (mg/ g min) and β (g/ mg), respectively.

Table 2 and Fig. 9 indicate the kinetic parameters for europium and strontium adsorption at 25 °C on the produced samples. As seen from the values of correlation coefficients (r^2), the pseudo-second-order kinetic model provided a significant and comparable correlation for the sorption of Eu (III) and Sr (II) ions. The selectivity of the proposed kinetic model is confirmed by the comparison of the evaluated adsorption capacity considering the pseudo-second-order equation (q_e) and that found experimentally (q_{exp}). It proposed that the rate-determining step is a chemical- process, and that adsorption involves valence forces throughout the electron sharing between the Eu(III) or Sr(II) ions and prepared phytomass materials. The nonlinear relationship between the plotted data of the intra-particle diffusion model and the value of 'C' calculated ($C \neq 0$) suggests that this model does not play a significant role in the adsorption of Eu(III) or Sr(II) ions as shown in Fig. 9, and thus is not valid for the kinetics of adsorption.

Initial ion concentration effect

At optimum experimental conditions, the effect of various initial concentrations (25–500 mg/L) of Eu(III) and Sr(II) was investegated. The data showed that increasing M^+ concentration improved the q_m of each metal ion onto the RM and N-RM adsorbents, whereas increasing M^+ concentration decreased the removal percent, as shown in Fig. 10. It is due to an increase in driving force as the M^+ concentration in the liquid phase rises, which causes an increase in contact, resulting in an increase in the connection between the sorption sites on the adsorbent's outer sphere and metal ions. [28]. The q_m of Eu(III) is 46.7 for N-RM and 16.4 mg/g for RM, respectively. While q_m for Sr (II) reaches about 10.41 and 8.87 mg/g on the RM and N-RM, respectively. At the same time, the phosphate negative charge on the surface of N-RM is normally surrounded by a counter ion cloud of M^+. The concentration and the size of the counter ions are the major factors influencing the adsorption process [29].

Equilibrium isotherm

The equilibrium of the process was described by Langmuir, Freundlich, and Dubinin-Radushkevich (D-R) isotherm models. According to Langmuir's isotherm model, monolayer sorption causes the uptake of homogenous surfaces with no interaction between sorbed molecules. The theory states that adsorption energies on the material are equal [28]. Freundlich's isotherm [30] is the first documented relationship that describes the sorption formula. This isotherm is valid for physical adsorption and usually for an adsorbent with a very heterogeneous surface [31]. The D-R isotherm model also considers a heterogeneous surface [32]. The formulas for the non-linear Langmuir and Freundlich isotherm models are shown in Eq. 7, 8, and 9:

$$\text{Langmuir isotherm} \quad q_e = \frac{q_m C_e K_L}{1 + K_L C_e} \tag{7}$$

$$\text{Freundlich isotherm} \quad q_e = K_f C_e^{1/n} \tag{8}$$

$$\text{The linear form of (D} - \text{R) isotherm} \quad Lnq_e = Lnq_m - \beta\varepsilon^2 \tag{9}$$

where C_e denotes the adsorbate's equilibrium concentration in solution (mg L^{-1}), q_e denotes the equilibrium adsorption capacity (mgg^{-1}), q_m denotes the sorbent's maximum

Table 2 Adsorption kinetic parameters for Sr(II) and Eu(III) adsorption on RM and N-RM at 25 °C and initial conc. 50 mg/l

Kinetic models	Parameters	Sr(II)		Eu(III)	
		RM	N-RM	RM	N-RM
Pseudo-first-order equation	$q_{e\ (exp.)}$(mgg-1)	1.4	2.4	4.39	4.80
	$q_{e\ (Cal.)}$ (mgg^{-1})	1.7	10.2	0.929	0.445
	K_1(min^{-1})	0.002	0.002	0.023	0.021
	R^2	0.847	0.680	0.841	0.959
Pseudo-second-order equation	$q_{e\ (Cal.)}$ (mgg^{-1})	1.43	2.41	4.46	4.81
	K_2 (min^{-1})	0.098	0.636	0.077	0.534
	R^2	0.999	1	0.999	1.000
Intra-particle diffusion	K_p (mgg^{-1} $min^{-1/2}$)	0.001	0	0.096	0.014
	C	1.02	2.33	3.2	4.6
	R^2	0.837	0.49	0.618	0.664
Elovich model	β (mg g^{-1} min^{-1})	1	1	2.58	16.9
	$\boldsymbol{\alpha}$ (g mg^{-1})	2.76	2.76	2.2	7.8
	R^2	0.837	0.490	0.804	0.862

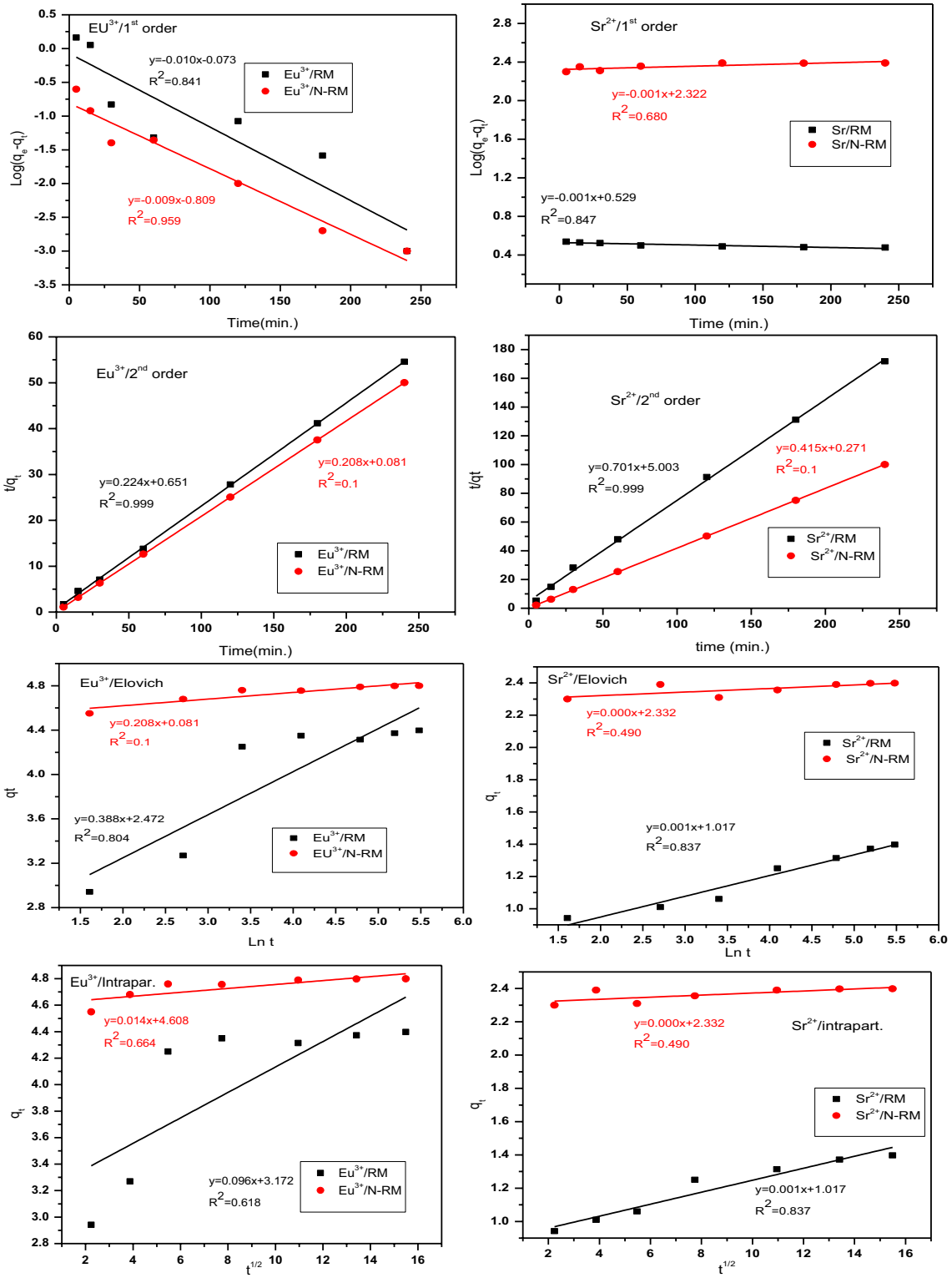

Fig. 9 Pseudo-first order, second order, Elovich, intra-particle diffusion kinetic modeling of Eu(III) and Sr(II) adsorption on RM and N-RM

adsorption capacity, and b denotes the affinity constant. The constant K_f denotes the sorbent's adsorption capacity (mg g^{-1}), while the constant n denotes the adsorption intensity. q_m is the highest sorption capacity, whereas β is a constant correlated to sorption energy. The following formula can be used to evaluate the, Eq. 10:

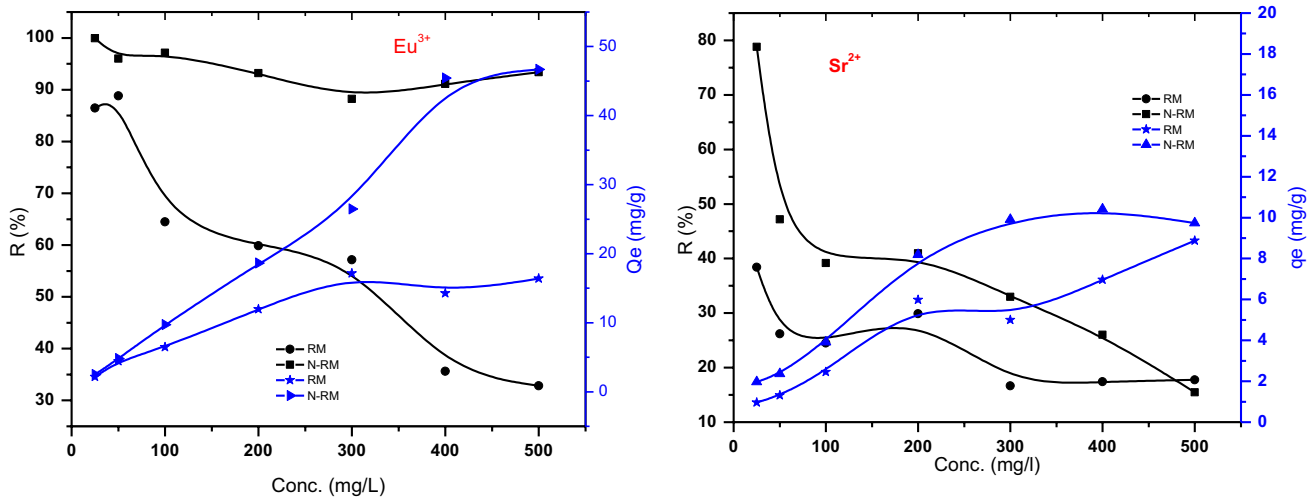

Fig. 10 The effect of initial metal ion concentration (Sr(II) and Eu(III)) on the removal % and maximum capacity at 25 °C

$$\varepsilon = RTLn\left(1 + \frac{1}{C_e}\right) \tag{10}$$

R (J.mol/K) is the gas constant, and T is the absolute temperature.The mean free energy of sorption (E) is the free energy that change when 1 M of ions are transferred to the adsorbent surface from an infinite solution. E is calculated from the β value using the following Eq. 11:

$$E = \frac{1}{\sqrt{2\beta}} \tag{11}$$

The data in E can describe the reaction mechanism. If E is in the range of 8–16 kJ/mol, sorption is governed by ion exchange. In the case of E < 8.0 kJ/mol, the sorption was physically controlled. If E > 16 kJ/mol, the M^+ was chemically adsorbed [33]. According to the data of this study, it was determined that the adsorption of Eu (III) and Sr(II) by both adsorbents was via ion-exchange and chemical reaction. From the experimental data, as shown in Fig. 11, the parameters of D–R, Freundlich, and Langmuir isotherms were calculated and summarized in Tables 3 and 4. The correlation coefficient (r^2) calculated for the sorption of Eu(III) ions onto the RM and nano-prepared material N-RM indicates that the obtained data is the best fit with those calculated by both Freundlich and Langmuir isotherms in the case of N-RM and D-R is more fit to the data in the case of RM materials understudied experimental conditions. In the case of RM, the experimental data of Sr (II) was fitted to D–R, Freundlich, and Langmuir isotherms. The Freundlich, and Langmuir isotherms fit the experimental data of strontium sorption on the N-RM. It was noted that the n values lie between 1 and 0, which indicates a favourable sorption process [34].

From Tables 3 and 4, it can be observed that the obtained values of mean D–R energy, E are 11.2 and 15.8 kJ/mol for Eu/RM and Eu/N-RM, respectively. The sorption of Eu(III) is clearly controlled by ion exchange reactions. The E values for Sr/RM and Sr/N-RM are 14.1 and 44.7 kJ/mol, respectively, indicating that ion exchange and/or chemisorption have played a dominant role in the mechanism of Sr(II) sorption onto the prepared materials. Similarly, [35] established that Adsorption is considered promising if the value of K_F is found in the range of 1–20, and results reveal that in the present study, K_F was 2.536, 1.25, 1.175, and 1.19 for Eu/RM, Eu/N-RM, Sr/RM, and Sr/N-RM, respectively. Therefore, by comparing, the order of the sorption capacity according to the Langmuir isotherm is Eu/N-RM > Eu/RM > Sr/N-RM > Sr-RM. These results show that Eu(III) and Sr(II) adsorbed onto N-RM with greater power than RM.

Effect of interfering ions on the removal of Eu(III), and Sr(II)

The effect of interfering ions from the reactor's structural materials that are expected to be passivated in acidic medium on the removal of Eu(III) and Sr(II) at two different pH values of 2 and 5 using RM and N-RM is shown in Fig. 12. The most well-known activation products, according to the literature are Fe(III), Cr(III), and Co(II) [36], so studying their effect as interfering ions on the removal of Eu(III) and Sr(II) is an important case, as is studying the act of the prepared adsorbents (RM and N-RM) towards them. *Sinu Chandran* clearified that, presently, in the moderator system of some 540 MWe PHWRs, nickel-based common alloys are being used, for the internals of valves and pump seals, to avoid the generation of ^{60}Co ($t^{1/2}$ = 5.27 years) from neutron-activation of corrosion products. But in certain off-normal conditions, corrosion of these valves was observed,

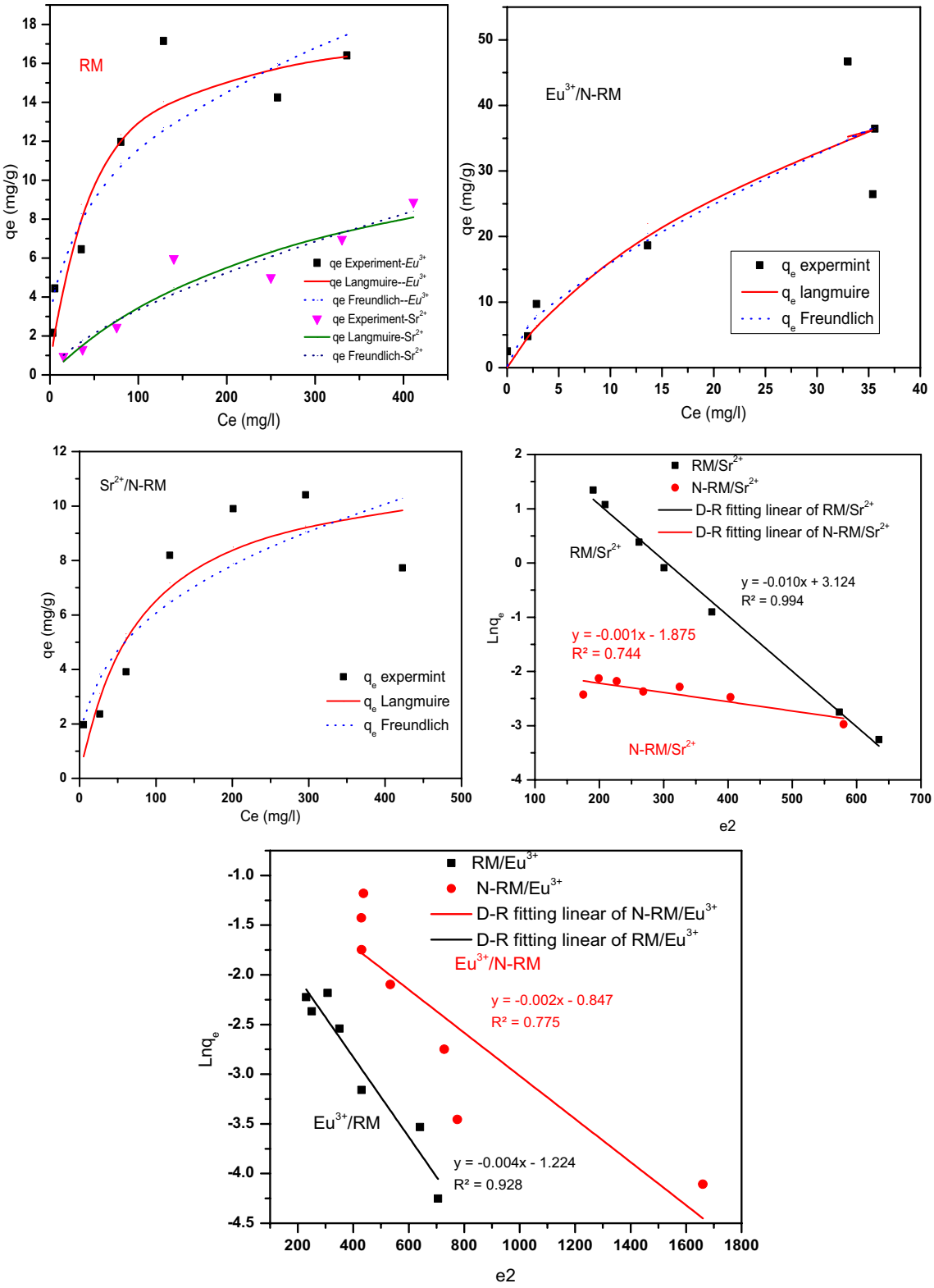

Fig. 11 Study the effects of different isotherms, non linear (Langmuir and Freundlich) and liner D-R models on the removal of Eu(III) and Sr(II) under optimal conditions

Table 3 Different adsorption isotherms parameter of Eu(III)sorption onto the prepared materials

Sorbent	Freundlich			Langmuir			
	$K_{f\ (mg/g)}$	n	R^2	$q_{max(mg/g)}$	b	R^2	$q_{exp.(mg/g)}$
RM	2.536	0.331	0.856	18.2	0.026	0.896	16.4
N-RM	1.25	0.602	0.848	60.4	0.041	0.846	46.7
	D-R						
	$q_{m\ (mol/g)}$		β		$E_{(KJmol-1)}$		R^2
RM	0.294		0.004		11.2		0.928
N-RM	0.428		0.002		15.8		0.755

Table 4 Different adsorption isotherms parameter of Sr(II)sorption onto the prepared materials

Sorbent	Freundlich			Langmuir			
	$K_{f\ (mg/g)}$	n	R^2	$q_{max(mg/g)}$	b	R^2	$q_{exp.(mg/g)}$
RM	1.175	0.642	0.983	11.5	0.003	0.982	8.87
N-RM	1.19	0.356	0.947	13.8	0.014	0.992	10.41
	D-R						
	$q_{m\ (mol/g)}$		β		$E_{(KJmol-1)}$		R^2
RM	0.02		0.01		14.1		0.994
N-RM	0.002		0.001		44.7		0.744

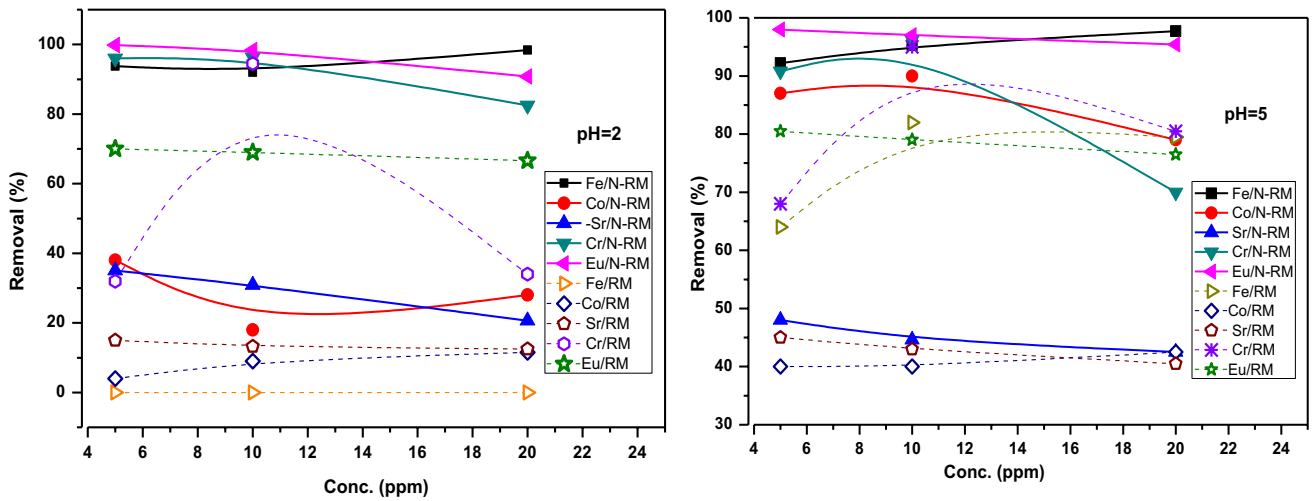

Fig. 12 Effect of interfering ions (Fe(III), Cr(III), Co(II)) on the removal of Eu(III) and Sr(II)at two different pH = 2, and 5

so there is a search for a better hard-facing alloy to withstand the erosion and corrosion in such an environment. The iron-based alloy SS–410, is being planned to be used in the internals of valves in place of colmonoy, as it is expected to have passivity in nitric acid medium.

It was discovered that functionalized Rose Mary with phosphate groups enhanced activation product removal, particullary for Fe(III), Cr(III) at pH = 2 and Fe(III), Cr(III), and Co(II) at pH = 5, without affecting Eu removal% and with a distinct change in the removal of Sr(II). This may be due to their large surface areas, accessible phosphorous active sites, controllable pore sizes and arrangements.

Varnali and Tiiziim-algan 1995 concluded that the anionic phosphate group was found to be the best site to bind

the divalent metal cations to form the most stable complexes. It was clear that the affinity of cations of the same charge to the RM and N-RM surfaces depends both on the nature of the adsorbing ion and the nature of the exchangeable cation on the surface. As the radius of an alkali earth M^+ decreases, so does its retention. Lanthanide ions adsorb in the same pattern across ion-exchange forms of RM and N-RM, with a rise in adsorption with a decrease in crystallographic radius, i.e., from La(III) to Lu(III). The exhibited laws are understood by considering that cation adsorption involves both electrostatic and extra-covalent donor–acceptor interactions between both the surface and the cations. The latter is related to the formation of -bonds between the electron pair in the interface of O_2 and the unoccupied p-, d-, or f-orbitals of adsorbing cations [37].

At both pHs, the uptake (%) of Cr(III) on RM appeared to increase with the initial M^+ concentration, reach a maximum (10 ppm), and then decline with further increases in the initial M^+ concentration. Because the carbon locations would eventually be filled with adsorbed Cr(III), adding more Cr(III) to the solution would not be expected to significantly increase the amount adsorbed. At increasing Cr(III) concentrations, the adsorbed M^+ may begin to resist each other, a concentration-dependent chemical conversion may occur, or diffusion effects may become more important [38]. The affinity of cations for cation exchangers increases with increased valence [39]. Therefore, the order of adsorption affinity of cations is as follows: monovalent ˂ divalent˂ trivalent. This explains why trivalence cations (Fe(III), Cr(III), and Eu(III)) have a higher removal rate than divalent cations (Sr(II), Co(II), and gives the authors reason to believe that N-RM can work as a cation exchanger resin. For cations of the same valence the adsorption affinity increases with decreasing radius, and according to Deby-Huckel Paraetr, the affinity depends on activity coefficient plots [39].

So, the reason that the trivalent cations including Cr(III) and Fe(III) have a greater affinity to adsorbents is because they have a smaller ionic radius than divalent cations Sr(II) and Co(II) (Fig. 12), because the sequence of affinity according to radius is Cr(III) (0.61 A) ˃ Fe(III) (0.64° A) ˃ Co(II) (0.74° A) ˃ Sr(II) (1.19° A)which is applicable in the present study.

Packets technique

This research looks at a novel application for the purification of liquid waste containing first and foremost europium and strontium, as well as a mixture of the two with some interfering ions (Fe(III), Co(II), and Cr(III)). These metal ions can be eliminated from waste water using a method that is simpler to use and more practical for waste treatment on a large scale. In the case of Eu(III), the R% using the packet containing RM decreased from 83% (as determined by the previous studied pH effect in Fig. 7) to 69.2% (as determined by packet sorption effect represent in Table 5). However, the R% using N-RM is remaining constant 95.6% (in both batch and packet sorption studies). Sr(II)'s R% using RM-containing packets has decreased from 27 to 18.8%, and its R% using N-RM packets has decreased from 48 to 44.2%. When the N-RM packets are immersed in a solution containing trivalent cation mixture of (Eu(III), Fe(III), and Cr(III) having R% (87.3, 99.5, and 97.3 correspondingly), it confirms their good performance. The defect in the shaking effect during the examined time may be connected to the drop in the R% of Eu(III) from 97 to 87.3, which can be treated by second-cycle operation.

The R% of Eu(III) in the case of the RM-packet immersed in a mixture of Fe(III), Sr(II), Co(II), and Cr(III) decreased sharply from 83% to 15.6%, complicating its use in the removal of only Eu(III) but approving its excellent adsorptive behavior towards Fe(III) and Cr (III).

Finally, this technology is highly helpful for usage in large-scale liquid radioactive waste, especially with packets containing N-RM. It can be employed for the first and second cycles for a maximum operation. A third cycle may be added to ensure that Sr(II) is completely removed from its interfering ions.

Comparison sorption capacity

The results revealed that RM and N-RM sorbent materials exhibited a good sorption capacity compared with other materials as reported in the literature (Table 6). From these results, we can conclude that the N-RM powder can be considered a promising material for the sorption of Sr(II) and Eu(III) from waste water.

Table 5 Removal% of Eu(III), Sr(II), Fe(III), Co(II), and Cr(III) according to packet technique

Adsorbents	Metal ions	Removal %				
		Fe(III)	Co(II)	Sr(II)	Eu(III)	Cr(III)
RM	Sr(II), Eu(III)	––	––	18.8	69.2	––
N-RM	Sr(II), Eu(III)	––	––	44.2	95.6	––
RM	Eu(III), Fe(III), Co(II), Sr(II), Cr(III)	92.4	30.5	10.7	15.6	96.3
N-RM	Eu(III), Fe(III), Co(II), Sr(II), Cr(III)	99.5	38	14.1	87.3	97.3

Table 6 A comparison of the q_{max} values obtained for Eu(III)and Sr(II) adsorption on the prepared RM and N-RM with other adsorbent materials

Adsorbent materials	Adsorption capacity (mg g^{-1})		References
	Eu(III)	Sr(II)	
Saccharomyces cerevisiae	14.2	–	[40]
Phalaris seed peel (PSP)	16.79	–	[41]
Egg shell Hyroxyapatite	–	47.7	[42]
Sodium montmorillonite (pH = 5)	–	41.49	[43]
Synthetic saponite (pH = 5)	–	26.6	[44]
Alumina-Zerconia-Ceria composite	–	2.61	[28]
Sawdust	2.4	–	[45]
Modified cellulose acetate	9.35	–	[46]
ZSM-5 zeolite	3.3	–	[47]
Nano-hydroxyapatite-fulvic acid	94.4		[20]
MnO(OH)-modified diatomite	10	17	[48]
modified activated carbon (coconut shell)	136.84	69.85	[49]
RM	18.2	11.5	This work
N-RM	60.4	13.8	This work

Conclusion

The phytomass residue of rosemary (RM) leaf seems to be an effective adsorbent in a batch system. It was modified using phosphoric acid to prepare nanomaterial (N-RM) with a pore size ˂50µ. Both adsorbents are used for the removal of Eu (III) and Sr (II). According to batch technique, the preferred pH is 5. The adsorption increased with shaking time and attained equilibrium after 60 and 15 min for RM and N-RM, respectively. According to (R^2), a pseudo-second-order kinetic model fits the experimental results better. The maximum capacities according to Langmuir were 18.2, 60.4, 11.5, and 13.8 mg/g for Eu/RM, Eu/N-RM, Sr/RM, and Sr/N-RM, respectively. Ion exchange and chemical reactions were the predominant mechanisms according to the D-R, Langmuir, and Freundlich models. The behavior of Eu (III) and Sr (II) towards interfering ions was investigated and found to have a strong affinity for the trivalent cations Fe (III), Cr (III), and Eu (III). Modified sorbents (N-RM) have higher surface stability of Eu(III) than RM, allowing them to be less affected by the presence of counter ions. A novel packet technique has excellent behavior towards trivalent cations and is recommended to be applied to scale up the process to an actual waste solution.

Funding The authors declare that no funds, grants, or other support were received during the preparation of this manuscript.

Availability of data and materials The data sets generated during and/or analyzed during the current study are available from the corresponding author on reasonable request.

Declarations

Ethical approval and Consent to participate Not applicable.

Consent for publication Not applicable.

Competing interests The authors declare that they have no competing interest.

References

1. Abdel Rahman RO, Zaki AA, El-Kamash AM (2007) Modeling the long-term leaching behavior of ^{137}Cs, ^{60}Co, and $^{152,154}Eu$ radionuclides from cement–clay matrices. J Hazard Mater 145:372–380
2. Zaki AA, El-Zakla T, Abed El Geleel M (2021) Modeling kinetics and thermodynamics of Cs^+ and Eu(III) removal from waste solutions using modified cellulose acetate membranes. J Membrane Sci 401–402:1–12
3. Sabriye YE, Sema E (2011) Adsorption characterization of strontium on PAN/zeolite composite adsorbent. J Nucl Sci Technol 1:6–12
4. Lehto J, Hou X (2011) Chemistry and Analysis of Radionuclides, Laboratory Techniques and Methodology, Wiley-VcH Verlag GmbH&Co.KGaA.
5. Abdelhady A (2013) Radiological performance of hot water layer system in open pool type reactor. J Alex Eng 52:159–162
6. Qu-Yang XK, Jin RN, Yang LP, Wen ZS, Yang LY, Wang YG, Wang CY (2014) Partially hydrolyzed bamboo (phyllostachys heterocycla) as a porous bioadsorbent for the removal of Pb (II) from aqueous mixtures. J Agric Food Chem 62:6007–6015
7. Hu XJ, Wang JS, Liu YG, Li X, Zeng GM, Bao ZL, Zeng XX, Chen AW, Long F (2011) Adsorption of chromium (VI) by ethylenediamine-modified cross-linked magnetic chitosan resin: Isotherms, kinetics and thermodynamics. J Hazard Meter 185:306–314
8. Amthor JS (2010) From sunlight to phytomass: on the potential efficiency of converting solar radiation to phyto-energy. New Phytol 188:939–959
9. Ozcan MM, Chalchat J-C (2008) Chemical composition and antifungal activity of rosemary (*Rosmarinus officinalis* L.) oil from Turkey. In J Food Sci Nutr 59:691–698
10. Genena AK, Hense H, Smania JA, de Souza SM (2008) Rosemary (Rosmarinus officinalis): a study of the composition, antioxidant and antimicrobial activities of extracts obtained with supercritical carbon dioxide. Food Sci Technol 28:463–469
11. Erhayem M, Al-Tohami F, Mohamed R, Ahmida K (2015) Isotherm, kinetic and thermodynamic studies for the sorption of mercury (II) onto activated carbon from Rosmarinus officinalis leaves. Am J Anal Chem 6:1–1
12. Amin MT, Alazba AA, Shafiq M (2017) Effective adsorption of methylene blue dye using activated carbon developed from the rosemary plant: isotherms and kinetic studies. Desalin and Wat Treat 74:336–345
13. Banuprabha TR, Karthikeyani A, Kalyani P (2021) Evaluation and application of phytomass derived activated carbons as electrodes for coin cell supercapacitors. Int J Electrochem Sci 16:211251. https://doi.org/10.20964/2021.12.21

14. Sun YP, Zhou B, Lin Y, Wang W, Fernando KS, Pathak P, Meziani MJ, Harruff BA, Wang X, Wang H (2006) Quantum-sized carbon dots for bright and colorful photoluminescence. J Am Chem Soc 128:7756–7757
15. Ingle PK, Karishma A, Rathod VK (2016) Copper removal using acid activated peanut husk from aqueous solution. J Environ Eng Landsc Manag 24(3):210–217. https://doi.org/10.3846/16486897.2016.1184151
16. Kokol V, Bozic M, Vogrincic R, Mathew AP (2015) Characterization and properties of homo- and heterogenously phosphorylated nanocellulose. Carbohyd Polym 125:301–313
17. Zhang Y, Zheng R, Zhao J, Ma F, Zhang Y, Meng Q (2014) Characterization of H_3PO_4-treated rice husk adsorbent and adsorption of Copper(II) from aqueous solution. Biomed Res Int. https://doi.org/10.1155/2014/496878
18. Oliveira GF, de Andrade RC, Aparecido M, Trindade G, Andrade HMC, de Carvalho CT (2017) Thermogravimetric and spectroscopic study (TG–DTA/FT–IR) of activated carbon from the renewable biomass source babassu. Artigo Quim Nova 40(3):284–292
19. Gad HMH, Youssef MA (2018) Sorption behavior of Eu(III) from an aqueous solution onto modified hydroxyapatite: kinetics, modeling and thermodynamics. Environ Technol 39(20):2583–2596
20. Imam DM, Youssef MA, Attallah MF (2020) Promising framework of nanocomposite materials: synthesis and radio-lanthanides labeling for nuclear medicine application. J Radioanal Nucl Chem 323:749–761
21. Yang P, Wei (2019) Novel nanomaterials for protein analysis, Chapter 2, Novel Nanomaterials for Biomedical, Enviro. and Energ. Applicat.
22. Liebmann P, Loew G, Mclean AD, Pack GR (1982) Ab initio SCF studies of interactions of lithium(+), sodium(+), beryllium(2+), and magnesium(2+) ions with dihydrogen phosphate(-) ion: model for cation binding to nucleic acids. J Am Chem Soc 104(3):691–697
23. Barrozo A, Blaha-Nelson D, Williams NH, Kamerlin SCL (2016) The effect of magnesium ions on triphosphate hydrolysis. J Pure Appl Chem 89(6):715–727. https://doi.org/10.1515/pac-2016-1125
24. Alkan M, Demirbas O, Alikcapa S, Dogan M (2004) Sorption of red 57 from aqueous solution onto sepiolite. Hazard Mater B 116:135
25. Ho YS, McKay G (1999) Pseudo-second order model for sorption processes. Process Biochem 34:451
26. Weber WJ, Morris JM (1963) Kinetics of adsorption of carbon from solutions, J Sanit Eng. Div Am Soc Eng 89:31
27. Teng H, Hsieh C-T (1999) Activation energy for oxygen chemisorption on carbon at low temperatures. Ind Eng Chem Res 38:292–297
28. Attallah MF, Hassan HS, Youssef MA (2019) Synthesis and sorption potential study of Al_2O_3-ZrO_2-CeO_2 composite material for removal of some radionuclides from radioactive waste effluent. Appl Radia Isotop 147:40–47
29. Weidlich T, Lindsay SM, Rupprecht A (1988) Counterion effects on the structure and dynamics of solid DNA. Phys Rv Lett 61:1674. https://doi.org/10.1103/PhysRevLett.61.1674
30. Freundlich H (1970) Uber die adsorption in losungen. Zeitschrift fur physikalische Chemie 57:385–470
31. Benes P, Majer V (1980) Trace chemistry of aqueous solutions. Elsevier, New York, NY
32. Bering B, Dubinin MSerpinsky V, (1972) On thermodynamics of adsorption in micropores. J of Colloi Interfa Sci 38:185–194
33. Derakhshani E, Naghizadeh A, Khodadadi M (2016) Application of different isotherm models for humic acid adsorption on to bentonite and montmorillonite nanoparticles. Health Scope 6(2):e40416
34. Goldberg S (2005) Equations and models describing adsorption processes in soils. Chemical processes in soils. Chapter 10, SSSA book series. Soil Science Society of America, Madison (WI)
35. Batool F, Akbar J, Iqbal S, Noreen S, Nasir S, Bukhari A (2018) Study of isothermal, kinetic, and thermodynamic parameters for adsorption of cadmium: an overview of linear and nonlinear approach and error analysis. J Bioinorgan Chem Appl. https://doi.org/10.1155/2018/3463724
36. Rogowska J, Olkowska E, Ratajczyk W, Wolska L (2018) Gadolinium as a New Emerging Contaminant of Aquatic Environments. Environ Toxicolog and Chemis 37(6):1523–1534
37. Barany S, Strelko V (2013) Laws and mechanism of adsorption of cations by different ion-exchange forms of silica gel. Adsorption 19(2–4):769–776
38. Lalvani SB, Wiltowsk T, Hübner A, Weston A, Mandich N (1998) Removal of hexavalent chromium and metal cations by a selective and novel carbon adsorbent. Carbon 36(7–8):1219–1226
39. Frederick CN (1949) Ion Exchange: theory and application. Academic Press Inc., New York, N. Y.
40. Arunraj B, Sathvika T, Rajesh V, Rajesh N (2019) Cellulose and Saccharomyces cerevisiae embark to recover europium from phosphor. Powder ACS Omega 4:40–952. https://doi.org/10.1021/acsomega.8b02845
41. El-khalafawy A, Imam DM, Youssef MA (2022) Enhanced biosorption of europium and cesium ions from aqueous solution onto phalaris seed peel as environmental friendly biosorbent: Equilibrium and kinetic studies. Appl Radi Isotop 190:110498
42. Elsanafeny HA, Abo Aly MM, Hasan MA, Lasheen YF, Youssef MA (2020) Synthesis and polymeric modification of hydroxyapatite from biogenic raw material for adsorptive removal of Co^{2+} and Sr^{2+}. J Radioanal Nucl Chem. https://doi.org/10.1007/s10967-020-07411-2
43. Hassan SSM, Kamel AH, Youssef MA, Aboterika AHA, Awwad NS (2020) Removal of barium and strontium from wastewater and radioactive wastes using a green bioadsorbent, Salvadora persica (Miswak). Desalinat and Wat Treatm 192:306–314
44. Guo Y, Hong Nhung NT, Dai X, He C, Wang Y, Wei Y, Fujita T (2022) Strontium ion removal from artificial seawater using a combination of adsorption with biochar and precipitation by blowing CO_2 nanobubble with neutralization. Front Bioeng Biotechnol 10:819407. https://doi.org/10.3389/fbioe.2022.819407
45. Hassan HS, Attallah MF, Yakout SM (2010) Sorption characteristics of an economical sorbent material used for removal radioisotopes of cesium and europium. J Radioanal Nucl Chem 286:17–26. https://doi.org/10.1007/s10967-010-0654-x
46. Zaki A, El-Zakla T, El Geleel MA (2012) Modeling kinetics and thermodynamics of Cs^+ and Eu^{3+} removal from waste solutions using modified cellulose acetate membranes. J Membr Sci 401:1–12. https://doi.org/10.1016/j.memsci.2011.12.044
47. Shao DD, Fan QH, Li JX, Niu ZW, Wu WS, Chen YX, Wang XK (2009) Removal of Eu(III) from aqueous solution using ZSM-5 zeolite. Micropor Mesopor Mater 123:1–9. https://doi.org/10.1016/j.micromeso.2009.03.043
48. Sofronov D, Rucki M, Varchenko V, Bryleva E, Mateychenko P, Lebedynskiy A (2022) Removal of europium, cobalt and strontium from water solutions using MnO(OH)-modified diatomite. J Environm Chem Engineer 10(1):10694
49. Moloukhia H , Hegazy WS , Abdel-Galila EA, Mahrous SS (2015) Removal of Eu^{3+}, Ce^{3+}, Sr^{2+} and Cs^+ ions from radioactive waste solutions by modified activated carbon prepared from coconut shells, J Sci Res Sci,32: part:1.